Synthesis of Ferrocene Based Schiff Bases Possessing Different Metal Ion Sensing Aptitude and Partaking Antimicrobial Activity

Saranya Dhasarathan, Selvaraj Shunmugaperumal, Kamatchi Selvaraj P.*

PG & Research Department of Chemistry, Government Arts College for Men (Autonomous), Nandanam, Chennai-600 035, Tamil Nadu, India.

Corresponding author: Kamatchi Selvaraj P., email: porbal96@gmail.com

Abstract. Schiff bases comprised of highly reactive ferrocene derivatives and normal aromatic moiety have been prepared successfully. Spectral variations noticed in the spectra of newly synthesized receptors for the addition of different metal ions discloses the multi metal ion sensing ability of the prepared sensors. Harmonization of Cu^{2+} ions with receptor originate as MLCT band in the visible region. Shrewdness made from the data obtained from cyclic voltammetry studies give an idea about the concentration of metal ions needed for effective sensing. *In vitro* antimicrobial studies and H- bond energy calculation for the interaction between the above sensory materials and proteins of selected microorganisms using molecular docking studies disclosures the antifungal activity of newly prepared materials.
Keywords: Unsymmetrical Schiff bases; ferrocene; cation sensors; azomethine; binding attitude; molecular docking.

Resumen. Bases de Schiff derivadas de grupos ferrocenilos altamente reactivos y grupos aromáticas fueron preparadas exitosamente. La habilidad de los sistemas como sensores para detectar diversos iones metálicos se vió en la variación de las características observadas en sus espectors. La interacción de iones Cu^{2+} con el receptor produce una banda MLCT en la región visible. Los estudios de voltametría cíclica indican la concentración de los iones metálicos necesaria para una detección eficiente. Estudios antimicrobianos *in vitro* y cálculos de la energía de puentes de hidrógeno para las interacciones entre los sensores (bases de Schiff) y las proteínas de microorganismos selectos, basados en estudios de acoplamiento molecular, confirman la actividad antifúngica de los nuevos compuestos reportados.
Palabras clave: Bases de Schiff asimétricas; ferroceno; sensores de cationes; azometino; capacidad de interacción; acoplamiento molecular.

Introduction

Heavy metal ions and microbe's persistence in the environment is responsible for the deterioration of the quality of ecological system. Separation of metals from multifaceted   solutions containing trace amount of metals is achieved by MRT-SPE technique (Molecular recognition technology solid phase extraction) [1]. Essential and non-essential (but harmful) metals may exist in industrial effluent, body fluid, residue of radioactive material and metallurgical extract. The metal to be targeted may have interference by the other highly active potential ions which demands selective identification and isolation techniques. Unadventurous

methods like sedimentation, inductively coupled plasma mass spectrometry and inductively coupled plasma atomic emission spectrometry required skilled technical operator and also they are time consuming. Accurate analysis requires selective and sensitive materials capable of giving changes in absorption or emission spectra, redox potential and other physical properties like resistance [2,3]. Chemosensor are employed in various field including analytical, environmental, catalysis, industrial and medical sciences [4] as they meet the above requirement due to the accompaniment of high detection limit, selectivity, and specificity [5].

Medicines comprise of mercury are of skin ointment, laxative, antiseptic, and dental amalgams. Insertion of Hg^{2+} ions in the body foils the function of neurological system, brain, and kidney [6]. Copper, an essential metal, regulates energy production in cells, mechanism of oxygen transfer and transduction of signals in biological functions of body system [7]. Surplus intake of copper leads to acute nausea, multiple organ failure, hike in blood pressure miscarriages and Alzheimer's diseases [8]. Plants and some microorganisms (algae, archaea, bacteria & primitive eukaryotes) contain nickel existing enzymes [9]. Existence of enzymes with nickel in higher organisms is not reported. Oral ingestion of nickel by human induces pathophysiological changes and causes genotoxicity, oxidative stress, lung fibrosis, cardiovascular diseases, immunotoxicity and cancer on the respiratory tract in living systems [10,11]. Sulphur containing enzymes having Ca^{2+} & Zn^{2+} ions are affected much by the category I carcinogens cadmium compounds. Accumulation of Cd^{2+} ions in biological system damages kidney, introduce cardiovascular disease and cancer [12]. Conservation of blood sugar, vitamin level, protection of immune and nerve cell functions are maintained by the manganese containing enzymes [13]. However, exposure to aerosols of Mn^{n+} or excess consumption of Mn^{2+} & Mn^{3+} containing component induces toxicity and affects brain, liver & cardio systems [14]. Non-biodegradable nature of lead makes it dangerous to human and living organisms [15]. Toxicity of lead includes kidney failure, neurotoxic effects including attainment of adolescence in children, shortfall of productivity and carcinogenic effect [16,17].

Embedded stability, aromatic nature, little toxicity and redox behavior of ferrocene-based complexes made them a gorgeous pharmacophore for drug design [18]. Coordination of ligated metal with ferrocene and its derivatives under different reaction conditions yielded complexes with fascinating redox processes and showing different measurable physical parameters like fluorescence. Further above type of complexes were found to have mixed properties of coordination complexes and organometallics [19]. Complexes derived with life essential metals like Co, Cu, Zn, Mn and Ni also showed antimicrobial activities when they are associated with heterocyclic molecules incorporated with N, O and S. It is reported that Schiff bases with benzimidazole moiety are sensitive to microbial agents and human pathogens [20].

Coordinating ability and biological activities of Schiff base ligands rest on the electron donating nature [21] of nitrogen atom (sp^2 hybridized) present in the imine groups. Present work discuss the synthesis of multi metal ion sensing, unsymmetrical, tetra dentate, Schiff base ligands *N'*1-((*E*)-4-(Nitro)benzylidene)-*N'*4-((*E*)-2-(ferrocenylidene)succinohydrazide and *N'*1-((*E*)-4-(Dimethylamino)benzylidene)-*N'*4-((*E*)-2-(ferrocenylidene)succinohydrazide along with their antimicrobial activity.

Experimental

Materials

Ferrocenecarboxaldehyde, P-dimethyl aminobenzaldehyde, 4-nitrobenzaldehyde, succinic anhydride, silica gel and hydrazinehydrate used in the synthesis of Schiff bases were purchased from E. Merck industry and are of analytical grade and used without purification. Chemicals like $CuCl_2$, $HgCl_2$, $Pb(OAc)_2$, $MnCl_2$, $NiCl_2$ and $Cd(OAc)_2$ utilized in CV and electronic spectral titration studies were of analytical grade and were obtained from Sigma–Aldrich. Acetonitrile (HPLC grade) got from E- Merck and absolute ethanol (spectral grade) acquired from Commercial Alcohols, Canada was employed for spectral studies. Supporting electrolyte tetrabutylammoniumperchlorate (99+% pure) was purchased from Chemical Center, Mumbai and employed without purification (with care).

Instruments

Mass spectrometer of model esquire 3000 obtained from Bruker Daltonics was employed to observe the mass spectra. For recording FTIR spectra with KBr pellets, in the range of 400-4000 cm^{-1}, Perkin-Elmer 337 spectrometer was utilized. Electronic spectral studies (in the range 200 to 800 nm) were carried out in SHIMADZU MODEL UV-1800 240V spectrophotometer. BRUKER AVANCE spectrometer operating at 500 MHz was tied up to register ^{1}H NMR spectra in C_2D_5OD solvent. Electrochemical analyses were done on CHI electrochemical analyzer 1200B model comprised of Ag/AgCl as reference electrode, glassy carbon as working electrode and platinum as counter electrode. Tetrabutylammonium perchlorate (0.1M) was used as supporting electrolyte under precautions in nitrogen atmosphere for CV studies. Responses to applied potential were recorded in acetonitrile medium (for $CuCl_2$, $NiCl_2$ and $HgCl_2$) and in ethanol medium (for $Pb(OAc)_2$, $MnCl_2$ and $Cd(OAc)_2$). Herarus C-H-N rapid analyzer was exploited to analyze the C, H and N contents of the receptors.

Synthesis of N'1-((E)-4-(nitro)benzylidene)-N'4-((E)-2-(ferrocenylidene)succinohydrazide [R1]

The precursor compound succinic acid dihydrazide was prepared by modifying the procedure reported in the literature [22]. To prepare succinic acid dihydrazide, solution containing 0.12 moles hydrazine hydrate in 150 ml of ethanol was added in drops along with stirring to a solution containing 0.05 moles of succinic anhydride in 50 mL of ethanol. The mixture was refluxed for 24 h. Precipitated product was dried and recrystallized from ethanol. Receptor compound was primed by adding a mixture containing 0.01 mole 4-nitrobenzaldehyde and 0.01mole of ferrocenecarboxaldehyde in 150 ml of ethanol to a solution having 0.01 mole of purified succinic acid dihydrazide in 50 ml of ethanol (scheme -1). Above mixture was stirred for half an hour and then refluxed for 6-7 h. Thin layer chromatographic technique was adopted to check the progress of the reaction at various time intervals. The reaction mixture was filtered after cooling and concentrated to get reddish yellow coloured *N'*1-((*E*)-4-(nitro)benzylidene)-*N'*4-((*E*)-2-(ferrocenylidene)succinohydrazide. Silica gel column was used to purify the crude sample by engaging ethanol as eluent. Colour: Dark reddish orange. Yield: 0.5939g (75%), m.p. 180 ℃.

Synthesis of *N'*1-((*E*)-4-(Dimethylamino)benzylidene)-*N'*4-((*E*)-2-(ferrocenylidene)succino hydrazide [R2]

Concoction containing 0.01 mole of ferrocenecarboxaldehyde and 0.01 mole of P-dimethyl amino benzaldehyde in 150 mL ethanol was added with stirring (half an hour) to a solution of 0.01 mole of succinic acid dihydrazide in 50 mL of ethanol (scheme -1). Above mixture was refluxed for 6-7 h. The progress of the reaction was checked by thin layer chromatographic technique at various time intervals. Cooled reaction mixture was filtered and concentrated. Red colored crude sample obtained was purified in a silica gel column using ethanol as eluent. Yield: 0.5805 g, (77 %), Color: reddish orange, m.p. 181 ℃.
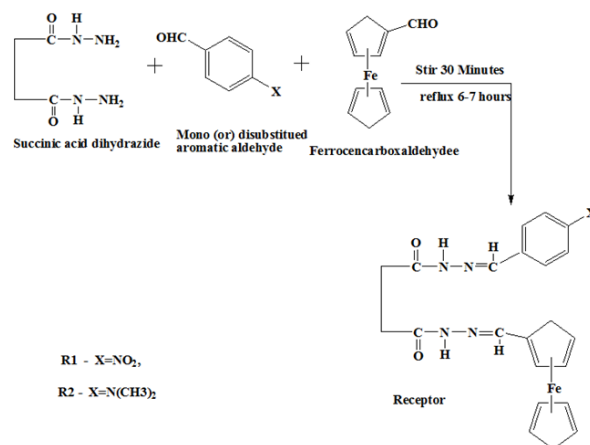
Scheme 1. Synthesis of Receptor R1 and R2.

Inhibition measurement against microorganisms (*In vitro*)

Adopting the procedure reported in the literature [23], experiments were carried out in triplicate against four bacteria and two fungi at appropriate temperature. Average values obtained from above experiments were considered for analysis. Each bacterial isolate was suspended in Brain Heart Infusion (BHI) broth and diluted to approximately 10^5 colony forming unit (CFU) per mL. They were flood-inoculated onto the surface of media (Mueller Hinton Agar for Bacteria and Sabouraud's Dextrose agar for fungi) and then dried. Five-millimeter diameter wells were cut from the agar using a sterile cork-borer and 30 µL (50µg compound in 500 µL DMSO) of the sample solution were poured into the wells. The plates were incubated for 18 h at 37 ºC for bacteria. Similarly fungal plates were incubated at room temperature (R.T) for 48 h.

Molecular docking method to estimate binding energy

The binding mode of synthesized compounds **R1** and **R2** with targeted proteins of the microorganisms were carried out using Auto dock version 4.2.6[24] running on windows 7. Targeted proteins were extracted from Research Collaboratory for Structural Bioinformatics (www.RCSB.org). Docking score values were calculated by employing molecular graphics laboratory (MGL) tools of Auto dock. Structures of **R1** and **R2** drawn using ChemSketch were converted to 3D structure with the help of 3D optimization tool.

Molecular Mechanics Force Field 94 (MMFF94) was used for geometrical optimization of ligands using ligand module. DFT - Quantum mechanics Geometry optimization using density functional theory (DFT) is done by moving the atoms of a molecule to get the most stable structure with the lowest possible ground state energy and therefore it is used for precise description of geometrical optimization. MMFF94 - Molecular mechanics ligands are considered to be fully flexible and some of the protein atoms are movable. The force field determines the energy of the protein-ligand complex for its every conformation. In this connect, DFT calculations are not carried out. The affinity of particular amino acid residue present in the selected protein with the synthesized ligands was done   and the H-bond interaction & binding energy (Kcal/mole) were calculated.

Results and Discussion

Characterization by Elemental and Mass Spectral Studies

The data arrived in elemental analysis matches very well with the theoretically calculated one: **R1-** $C_{22}H_{21}N_5O_4Fe$ (Found %): C, 55.65; H, 4.39; N, 14.70; Fe, 11.41; (Cal. %): C, 55. 60; H, 4.43; N, 14.76; Fe, 11.45). **R2-** $C_{24}H_{27}N_5O_2Fe$ (Found %): C, 61.10; H, 5.68; N, 14.79; O, 6.71. (Cal. %): C, 61.15; H, 5.72; N, 14.83; O, 6.77.

Advent of molecular peak (ESI) m/z at 474 and 472 for *N'*1-((*E*)-4-(Nitro)benzylidene)-*N'*4-((*E*)-2-(ferrocenylidene)succinohydrazide   and   *N'*1-((*E*)-4-(Dimethylamino)benzylidene)-*N'*4-((*E*)-2-(ferrocenylidene)succinohydrazide respectively on mass spectral analysis confirm the formation of expected receptors.

FTIR Spectral analysis

Peaks observed for **R1** around 475 cm^{-1} and 818 cm^{-1} are assigned for tilt stretching vibration of ferrocene cyclopentadienyl ring and C-H out of plane bend vibration respectively. Cyclopentadienyl ring -C-C-H bending vibrations appeared between 937 cm^{-1} to 1210 cm^{-1} [25]. The peak at 1393 cm^{-1} is allocated for symmetric stretching vibrations of -NO$_2$; 1515 cm^{-1} is allotted for -CH=N (imine) stretching vibration; 1667 cm^{-1} is dispensed for amide -C=O stretching vibration [26]. Peaks responsible for stretching vibration of secondary amine and water of hydration are seemed near 3080 cm^{-1} and 3200 cm^{-1} correspondingly (Fig. 1). For compound **R2** in addition to the above-mentioned peaks, the stretching vibrational modes in CH$_3$ groups are observed at 2932 cm^{-1} [27].
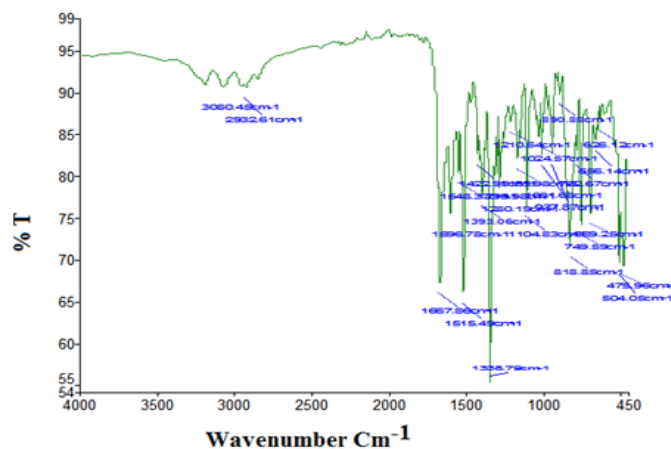
Fig.1. FTIR spectrum of compound **R1**.

NMR Spectral analysis

The ¹H NMR spectra of the synthesized sensors were recorded after dissolving them in C_2D_5OD solvent using 500 MHz frequency spectrometer. The peaks bestowed in the proton NMR spectrum of **R1** are assigned accordingly δ,(ppm); 8.1(s, 2H, NCH), 7.3 (m, 4H, aromatic), 4.5 (m, 2H, cp subst), 4.3(m, 2H, cp subst), 4.1 (s,5H, cp unsubst), 2.8 (2s, 4H, $2CH_2$), 1.4(s, 2H, 2NH) (Fig. **2(a)**). For **R2** (Fig. **2(b)**) assignments are δ, (ppm); 8.4(s, 2H, NCH), 7.5 (m, 4H, aromatic), 4.3 (m, 2H, cp subst), 4.5(m, 2H, cp subst), 4.2 (s, 5H, cp unsubst), 2.7 (2s, 4H, $2CH_2$), 1.5(s, 2H, 2NH), 3.3 (2s, $6H-2CH_3$).
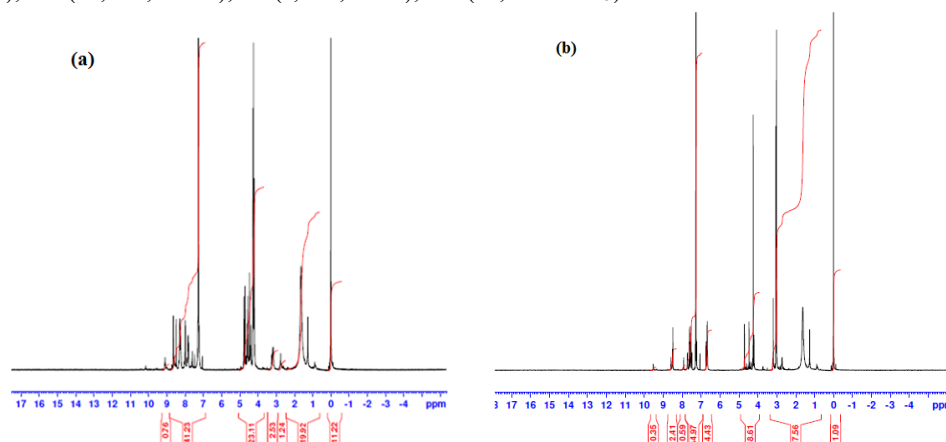

Fig.2. Proton NMR spectrum of **(a) R1** and **(b) R2**.

Assessment of detecting ability of sensors

UV-Visible titration method was utilized to assess the ability of newly synthesized sensor materials to detect several metal ions. Receptor solution of $1X10^{-5}$ M concentration (2.5 mL) was taken in the quartz cell. Twenty μL of $1X\ 10^{-2}$ M metal salt solutions were added up to seven additions and the spectral changes were recorded. The difference in solubility of metal salts split titration studies into two parts. Ethanol medium was engaged for salts of Mn, Pb and Cd. For Cu, Ni and Hg salts acetonitrile medium was employed.

Two shoulders near 241 nm & 322 nm and a broad peak around 297 nm (Fig. 3**(a)**) were noticed for **R1** in acetonitrile medium. Likewise two shoulders close to 233 nm & 420 nm and a wider peak at 306 nm were perceived (Fig. 3**(b)**) for **R1** in alcohol. UV- province peak and shoulders are earmarked for aromatic ring π-π* transition [28]. The visible region peak is assigned for d-d transition [29].
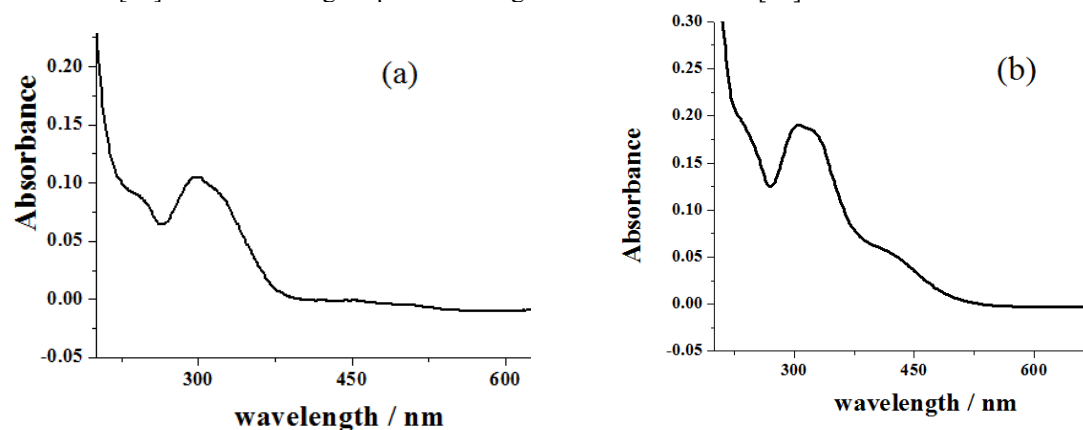

Fig. 3. Electronic spectra of **R1** in **(a)** acetonitrile **(b)** ethanol.

Successive addition of Cu^{2+} ions to receptor solution roots to the disappearance of the shoulder existing at 241 nm (Fig.4**(a)**), red shift of 297 nm broad peak to prominent peak around 308 nm, development of new shoulder near 354 nm at the expenses of 322 nm shoulder (Fig.4**(b)**) and formation of MLCT band, associated with the coordination of metal ion with sensor, around 458 nm (Fig.4**(c)**) which exposes sensing behavior of compound R1[30].
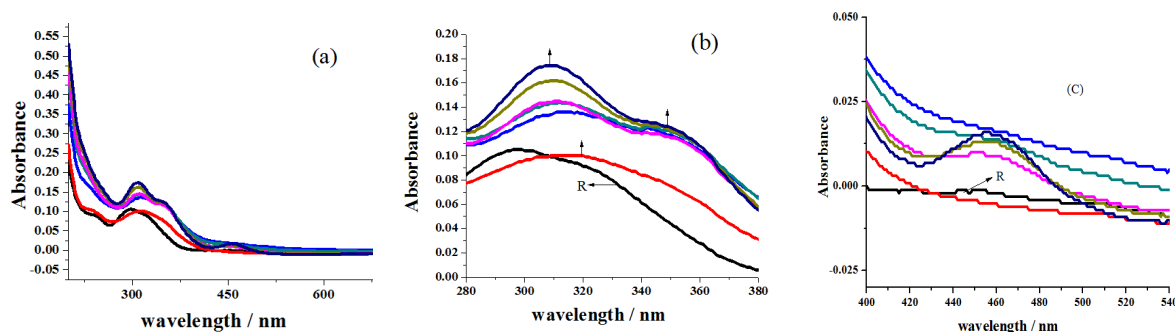

Fig. 4. Spectral changes noticed for the addition of Cu^{2+} ions **(a)** overall changes **(b)** redshift with new shoulder development **(c)** formation of MLCT band.

Cumulative additions of, Hg^{2+} ions causes conversion of 241 nm shoulder in to sharp peak at 235 (Fig. 5**(a)**); Ni^{2+} ions changes the 297 nm broad peak into shoulder near 309 nm (Fig. 5**(b)**); Pb^{2+} ions leads to the transformation of 233 nm shoulder into protuberant peak at 234 nm (Fig. 5**(c)**) projected the sensing ability of **R1**. Increasing the concentration of Mn^{2+} and Cd^{2+} ions into the receptor solution increases the absorbance value in all wavelength regions which also advocate the sensing behavior of **R1**[26].
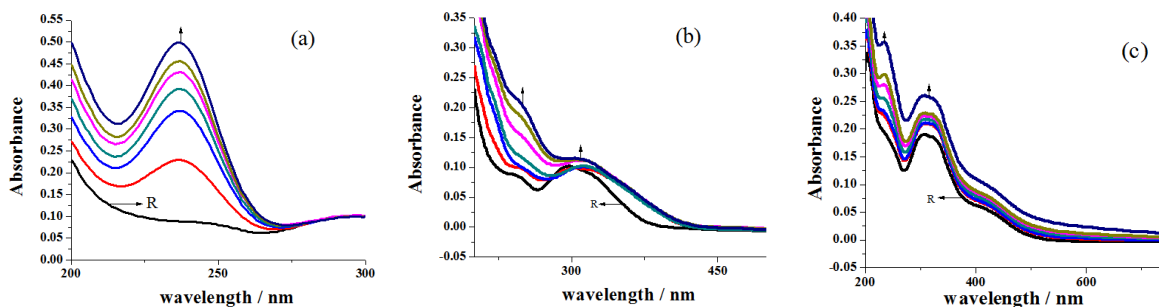
Fig. 5. Generation of new peaks for the addition of **(a)**Hg^{2+} ions **(b)** Ni^{2+} ions **(c)** Pb^{2+} ions.

Compared to **R1**, protruding peaks are observed for **R2** (Fig. 6**(a)** and 6**(b)**). Electron donating methyl groups present in the aromatic moiety of **R2** might have caused the n-π* transition to occur effectively, which in turn causes the appearance of prominent peaks in the spectrum of **R2**.

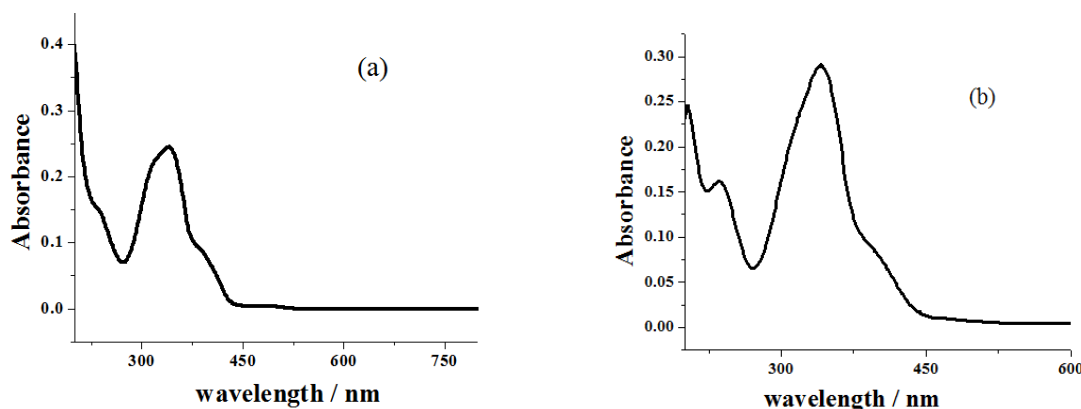**Fig. 6.** Electronic spectrum of **R2** in **(a)** acetonitrile **(b)** ethanol.

Formation of MLCT band [30] accountable for the association of sensor with metal ion around 461 nm (Fig. 7**(b)**), blue shift of 340 nm broad peak to 335 nm (Fig. 7**(c)**) with the disappearance of 235 nm and 385 nm shoulders (Fig. 7**(a)**) of receptor for the incremental addition of Cu^{2+} ions to **R2** discloses the sensing ability of receptor.
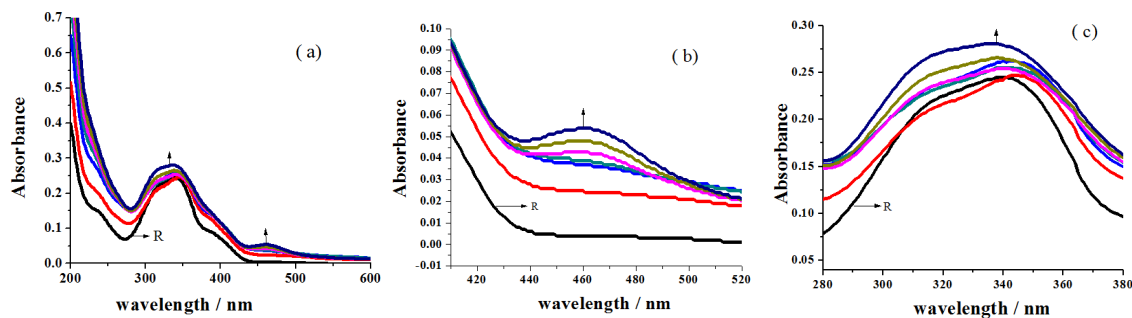

Fig. 7. Changes in the spectral behavior of **R2** for the addition of Cu^{2+} ion **(a)** overall changes **(b)** MLCT band formation **(c)** blue shift of broad peak.

349

Additions of, Hg^{2+} ions originate new peak at 239 nm (Fig.8**(a)**), Ni^{2+} ions leads to red shift of 340 nm broad peak to 350 nm (Fig.8**(b)**) and Pb^{2+}, Mn^{2+} including Cd^{2+} ions increase the absorbance throughout the wavelength region. Above observations substantiate the sensing behavior of **R2** towards different metal ions.
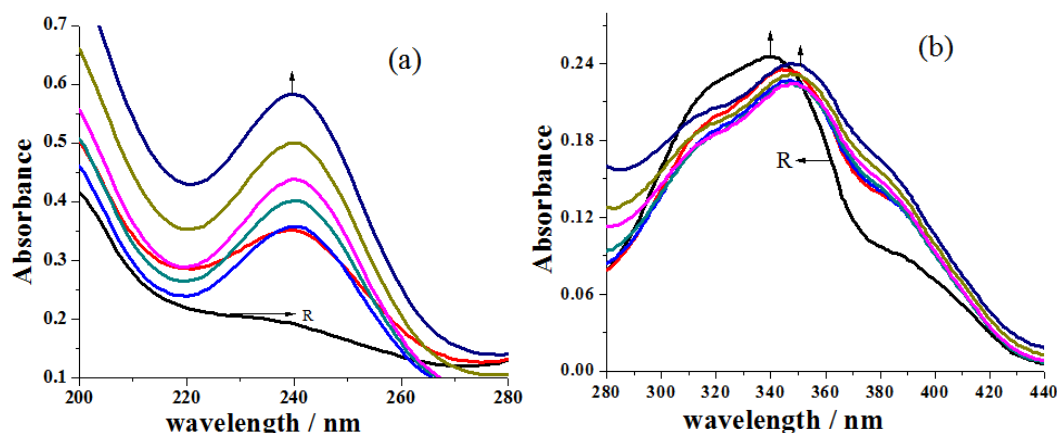

Fig. 8. Transformation of spectrum of **R2** for the addition of **(a)** Hg^{2+} ion **(b)** Ni^{2+} ions.

Responses to applied potential and its correlation with sensing ability

The cyclic voltammograms documented for **R1** under various scan rate (Fig. 9**(a)** and 9**(b)**) comprised oxidation peak near 0.685 V alongside reduction peak around 0.558 V [31]. Parameters like ΔE$_P$, I$_{pa}$ and I$_{pc}$ (Table 1) calculated from the voltammograms show raising trend with scan rate. The difference between the anodic and cathodic potential noticed (ΔE$_P$) falls in the range of 125 - 163 mV which propose quasi-reversible reduction of ferrocene moiety [32], as it is very high than the expected 59 mV of reversible process.
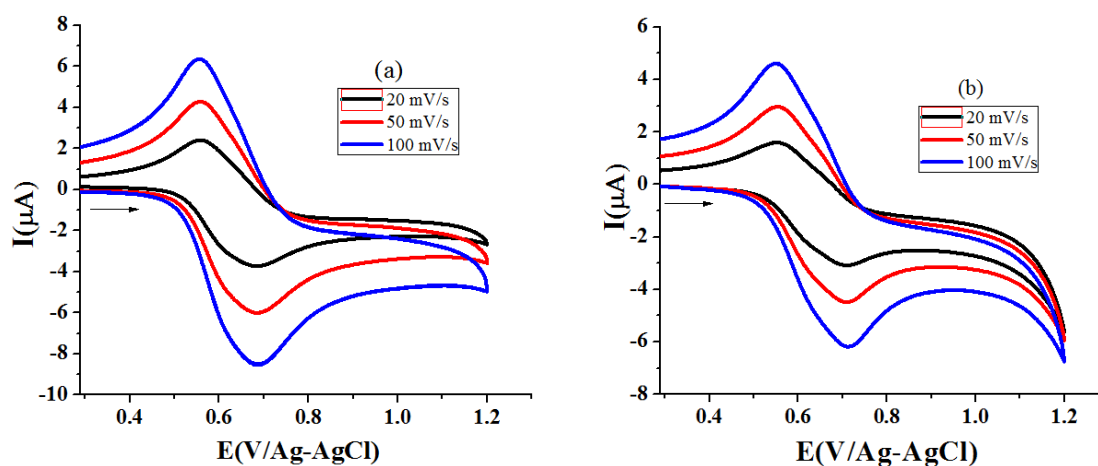

Fig.9. Voltammograms for **R1** under various scan rate **(a)** acetonitrile **(b)** ethanol.

Table 1. Electrochemical parameters for **R1**.

Scan Rate- mV/ sec	E_{pa} (V)	E_{pc} (V)	ΔE_p (V)	$E_{1/2}$ (V)	$I_{pa} \times 10^{-6}$ (µA)	$I_{pc} \times 10^{-6}$ (µA)
Solvent –Acetonitrile						
20	0.683	0.558	0.125	0.620	-3.787	2.415
50	0.685	0.558	0.127	0.621	-6.120	4.394
100	0.685	0.553	0.132	0.619	-8.638	6.416
Solvent – Ethanol						
20	0.706	0.558	0.148	0.632	-3.167	1.623
50	0.712	0.551	0.161	0.631	-4.563	3.019
100	0.712	0.549	0.163	0.630	-6.242	4.661

Redox behavior of ferrocene moiety after the addition of 20 µL (using micro pipette) of 1×10^{-3} M (Fig. 10(**a**)) or 1×10^{-1} M (Fig. 10(**b**)) metal salts solutions up to 7 equivalents to 10 ml of 1×10^{-3} M **R1** solution under 50mV/s scan rate demonstrate positive potential shift for oxidation peak and negative potential shift for reduction peak. Voltammograms obtained for the addition of Mn^{2+} ions to **R1** solution are presented below as an example.
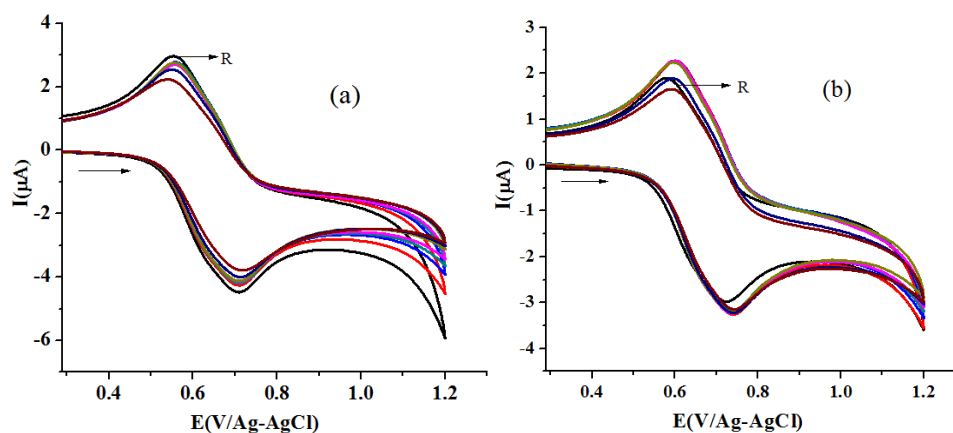
Fig. 10. Vicissitudes in voltammgram of **R1** for the addition of Mn^{2+} ions (**a**) 1×10^{-3} M, (**b**) 1×10^{-1} M.

Contact between the metal ions and receptor leads to changes in the redox peak of ferrocene moiety. It is reflected in the noticed ΔE_P and I_{pa} values. Electrochemical data taken for the successive addition of equimolar concentration of Cu^{2+} ions to **R1** is presented in Table 2.

Table 2. Electrochemical data for the addition of 1×10^{-3} M Cu^{2+} ions to 1×10^{-3} M **R1** solution (50 mv/s scan rate).

Addition	E_{pa}	E_{pc}	ΔE_p	$E_{1/2}$	$I_{pa} \times 10^{-5}$	$I_{pc} \times 10^{-6}$
Receptor	0.635	0.587	0.048	0.611	-3.732	2.637
20µL	0.625	0.674	0.049	0.649	-3.806	2.508
40µL	0.631	0.676	0.045	0.653	-3.59	2.854
60µL	0.633	0.679	0.046	0.656	-3.870	2.233
80µL	0.624	0.670	0.046	0.647	-3.733	2.919
100µL	0.620	0.681	0.061	0.650	-3.806	2.233
120µL	0.620	0.676	0.056	0.648	-3.532	2.919
140µL	0.622	0.683	0.061	0.652	-3.870	2.508

Dissimilarity in the binding affinity of different metal cations to sensor material is reflected in the noticed I_{pa} values (Table 3) for the addition of unalike metal ions ($1x10^{-3}$ M) to receptor solution ($1x10^{-3}$ M) (Fig. 11**(a)** and 11**(b)**). The repulsive force operating between the sensed metal cation and oxidized ferrocene moiety is also one of the reasons for the variation to occur in the noticed I_{pa} data [33]. Preference of recognizing order of **R1** arrived from the ΔI_{pa} % values intended from the Ipa statistic perceived for sensor solution and several metal ions added sensor solution is Hg-19.6 > Pb -15.9 > Ni-14.6 > Cu-8.7 > Mn -8.6 > Cd-2.9.
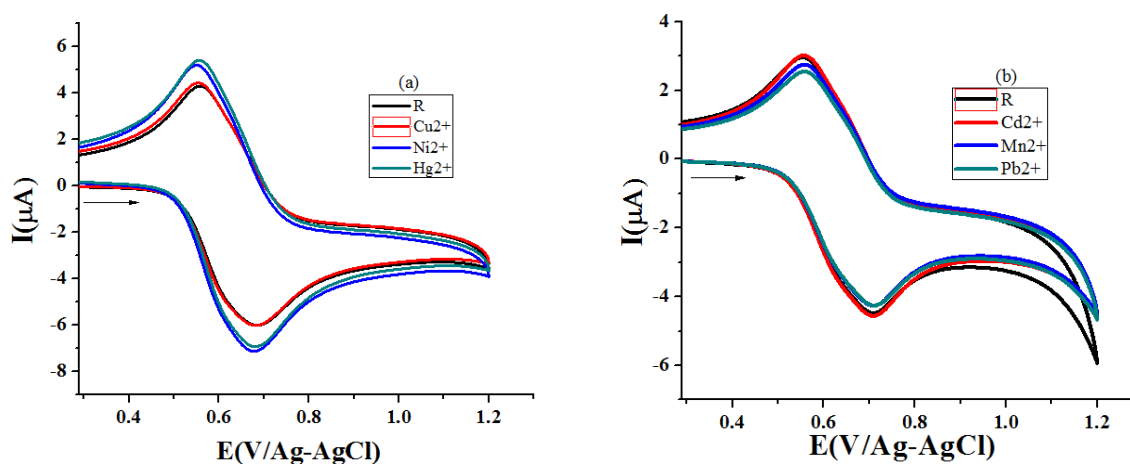

Fig. 11. Voltammograms recorded (scan rate- 50 mV/s) for the addition of different metal ion to **R1(a)** acetonitrile **(b)** ethanol.

Table 3. CV data for the addition of various metal ion solution (**R1**, 10^{-3} M / M^{2+}, 10^{-3} M) (Scan Rate-50 mV/sec).

Addition	E_{pa} (V)	E_{pc} (V)	ΔE_p (V)	$E_{1/2}$ (V)	$I_{pa} x10^{-6}$ (μA)	$I_{pc} x10^{-6}$ (μA)
Solvent - Acetonitrile						
Receptor	0.685	0.558	0.127	0.621	-6.120	4.394
Cu^{2+}	0.679	0.553	0.126	0.616	-5.992	4.433
Ni^{2+}	0.673	0.553	0.12	0.613	-7.188	5.151
Hg^{2+}	0.677	0.555	0.122	0.616	-6.949	5.470
Solvent - Ethanol						
Receptor	0.712	0.551	0.161	0.631	-4.563	3.019
Cd^{2+}	0.706	0.553	0.153	0.629	-4.629	3.112
Mn^{2+}	0.712	0.558	0.154	0.635	-4.274	2.758
Pb^{2+}	0.708	0.558	0.15	0.633	-4.329	2.538

Sensing power of **R1** ($1x 10^{-3}$ M), under higher concentration of metal salts solution ($1x 10^{-1}$ M), deliberated (ΔI_{pa} %) from the I_{pa} values (Table-4) is Cd - 42.9 > Mn-26.1 > Pb-22.6 > Cu-14.6 >Hg-11.9 Ni-1.5. Comparison of ΔI_{pa} % amount attained for homo molar and hetero molar addition of metal salt solution exposes that **R1** has better sensing ability at higher concentration of metal salts. Further, **R1** is powerful towards Cd, Mn and Pb at higher concentration. It is potent to Hg, Pb and Ni at lower concentration. Fig. 12 represents the comparison made between the concentration of metal ions added and binding aptitude of **R1**.
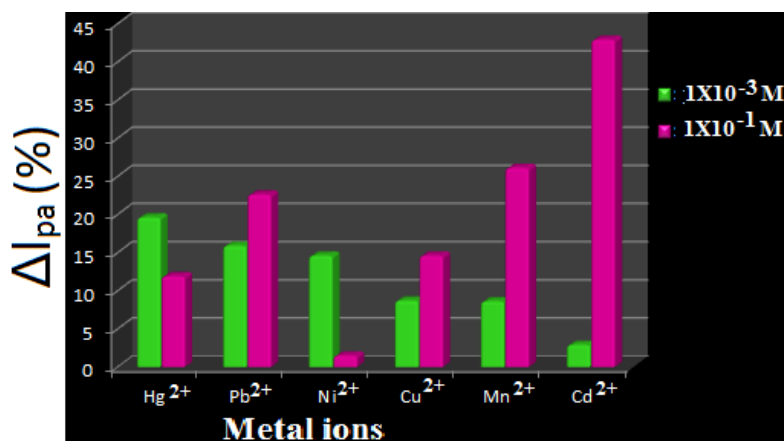
Fig.12. Comparison chart for sensing ability of **R1**.

Table 4. Electrochemical data obtained for the addition of $1X10^{-1}$ M metal salt solutions to $1X10^{-3}$ M **R1** (scan rate- 50 mV/s).

Addition	E_{pa} (V)	E_{pc} (V)	ΔE_p (V)	$E_{1/2}$ (V)	I_{pa} x10^{-6} (µA)	I_{pc} x10^{-6} (µA)
Solvent - Acetonitrile						
Receptor	0.685	0.558	0.127	0.621	-6.120	4.394
Cu^{2+}	0.727	0.613	0.114	0.67	-7.906	5.151
Ni^{2+}	0.725	0.609	0.116	0.667	-7.587	4.391
Hg^{2+}	0.739	0.624	0.115	0.681	-6.912	4.991
Solvent - Ethanol						
Receptor	0.712	0.551	0.161	0.631	-4.563	3.019
Cd^{2+}	0.727	0.580	0.147	0.653	-3.074	1.721
Mn^{2+}	0.739	0.601	0.138	0.67	-3.266	2.229
Pb^{2+}	0.754	0.607	0.147	0.680	-3.540	2.336

Electron donating methyl groups present in the aromatic moiety might have played role in the response showed by **R2** for the applied potential and the voltammograms of **R2** entail three redox peaks (Fig. 13**(a)** and 13**(b)**) under all scan rates. The metal centered redox peak perceived near 0.67V is assigned for the electrochemical behavior of Fe(II) present in the ferrocene moiety [32]. Ligand centered electron transition between aromatic moieties of receptor and azomethine group [28] emerges about 0.91 V. The redox peak appeared around 1.25V may be earmarked for electrochemical reversible reduction of imine group [34,35].

The sensing performance of **R2** towards various metal ions was investigated using the same procedure used for **R1**. Figure 14**(a)** and 14**(b)** symbolize the changes in voltammograms noticed when 20 µL of HgCl$_2$ salt solution with different concentration (either $1X10^{-3}$ M or $1X 10^{-1}$ M) was added to 10 ml of $1X10^{-3}$ M receptor solution taken in the three compartment cell.
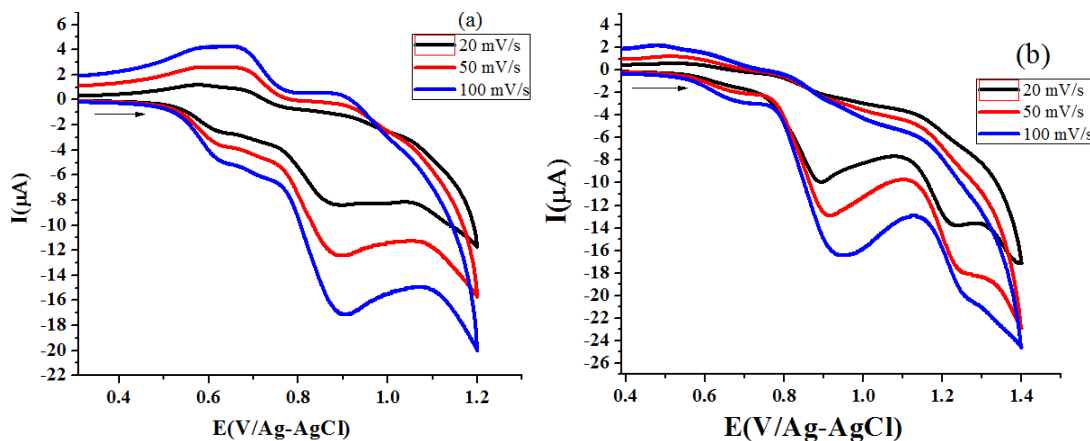
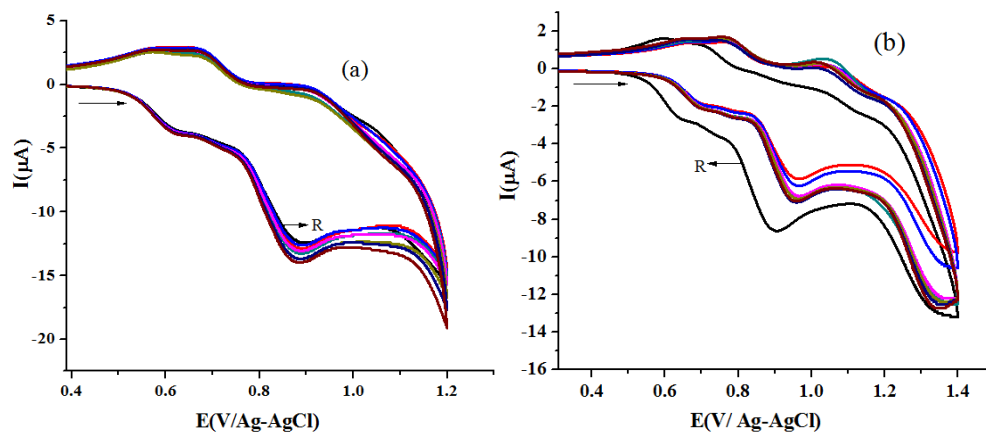**Fig. 13.** Voltammograms of **R2** with different scan rate in **(a)** acetonitrile, **(b)** ethanol.

Fig. 14. Change in voltammogram of **R2** for the addition Hg^{2+} ions **(a)** 10^{-3} M **(b)** 10^{-1}M.

Different I$_{pa}$ amount (Table 5) detected for dissimilar metal salt solution addition (20µL of 1X10^{-1} M) to **R2** solution (1X10^{-3} M) (Fig. 15**(a)** and15**(b)**) reflect the disparity in sensing aptitude of **R2**.

Table 5. Electrochemical data for hetero molar titration (**R2**, 10^{-3} M / M^{2+}, 10^{-1} M) (50 mV/ sec).

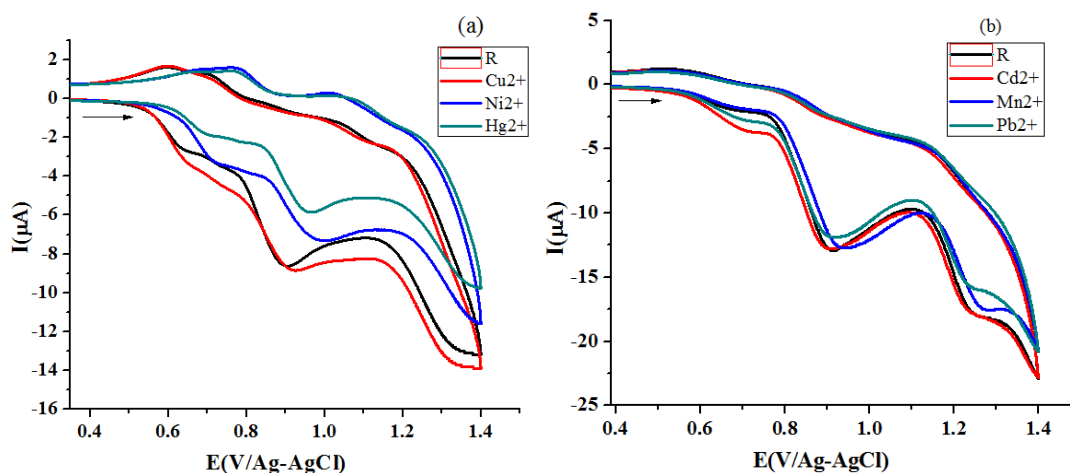| Addition	E$_{pa}$ (V)	E$_{pc}$ (V)	ΔE$_p$ (V)	E$_{1/2}$ (V)	I$_{pa}$ x10^{-6} (µA)	I$_{pc}$ x10^{-6} (µA)
Solvent - Acetonitrile						
Receptor	0.635	0.587	0.048	0.611	-3.732	2.637
Cu^{2+}	0.641	0.598	0.043	0.619	-3.1290	1.707
Ni^{2+}	0.699	0.704	0.005	0.701	-2.939	1.562
Hg^{2+}	0.690	0.770	0.08	0.73	-1.853	1.373
Solvent - Ethanol						
Receptor	0.659	0.532	0.127	0.595	-1.812	1.302
Cd^{2+}	0.707	0.541	0.166	0.624	-3.630	1.164
Mn^{2+}	0.682	0.521	0.161	0.601	-1.756	1.085
Pb^{2+}	0.709	0.518	0.191	0.613	-2.961	1.085

Fig. 15. Variations in CV of **R2** [scan rate -50 mV/s] for the addition of different metal ion **(a)** acetonitrile **(b)** ethanol.

CV titration studies under homo molar conditions (addition of 20μL $1X10^{-3}$ M metal salt solution to 10 ml of $1X10^{-3}$ M receptor solution) also displayed difference in perceived I_{pa} values for Cu, Ni and Hg salt solution addition. For Pb, Cd and Mn salt solution addition the behavioral changes in the voltammograms are not appreciable, which indicate that the concentration of metal ions is too low for the receptor **R2** to recognize them. The spot out ability of **R2** arrived from ΔI_{pa} values at multi molar concentration condition is Hg-47.9 > Ni-40.7 > Cu-35.2 >Mn-16.6 > Pb-16.6 > Cd-10.5 and at homo molar concentration it is (Cu-10.5>Hg-7.7>Ni1.2). The bar chart representation of role of concentration of metal ion and sensing ability **R2** is given in Fig. 16.
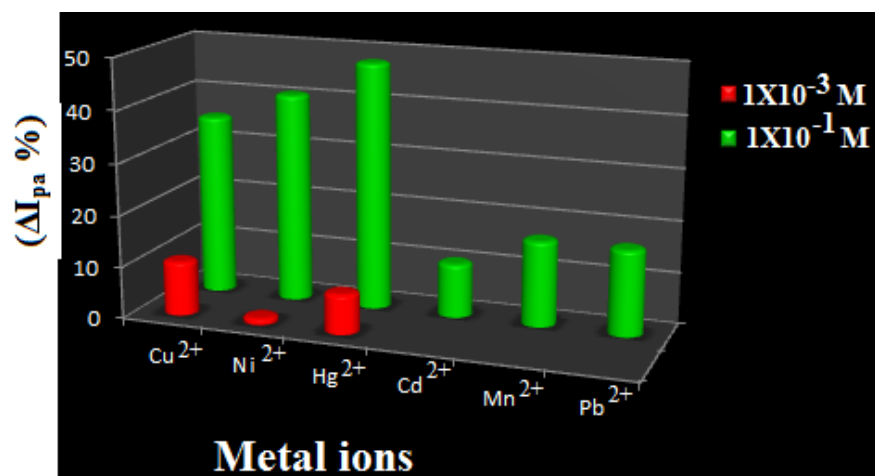

Fig. 16. Comparison chart for sensing ability of **R2**.

Impedance measurement for receptors solution (**R1** and **R2**) as well as Cu^{2+} ions ($1x10^{-3}$ M and $1x10^{-1}$ M) added receptor solution were measured. The Nyquist Plots (Fig. 17) arrived are presented here to support our investigation.
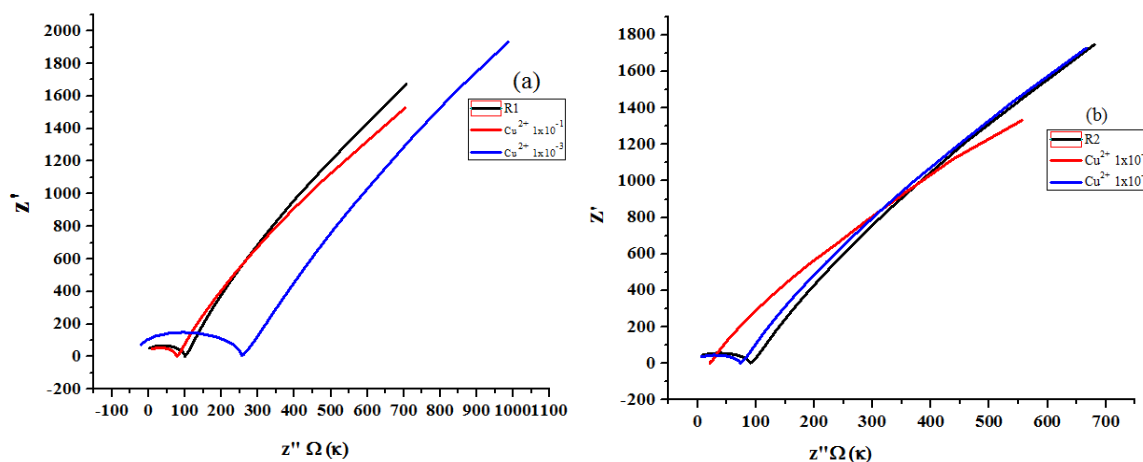
Fig. 17. Nyquist Plot for (a) **R1** and (b) **R2** with and without added Cu^{2+} ions.

In the comparison chat for sensing ability of **R1** (discussion section) it is proposed that **R1** sensing ability towards copper increases with increase in concentration of Cu^{2+} ions. In the impedance plot (Fig. 17**(a)**) R_{ct} value (260.7ohms) for 10^{-3} M Cu^{2+} ion added solution varies towards positive value compared to the R_{ct} value of **R1** (105.1 ohms), whereas for 10^{-1} M Cu^{2+} ion added solution the difference in R_{ct} value (79.2 ohms) is towards negative side. Similarly, on analyzing the comparative chat of **R2**, it is declared that **R2** is more potent at higher concentrations of Cu^{2+} ions. Impedance plot (Fig. 17**(b)**) of **R2** (R_{ct}- 90.3 ohms) shows minimum shift of R_{ct} value (72.3 ohms) for 10^{-3} M Cu^{2+} ion added solution and maximum negative shift of R_{ct} value (21.5 ohms) for 10^{-1} M Cu^{2+} ion added solution. Above observation ascertain that **R2** require high concentration of Cu^{2+} ion for effective sensing.

Antimicrobial Studies

Inhibition zone detected in antibacterial studies for **R1** & **R2** using disc diffusion method containing Mueller Hinton Agar base against *Escherichia coli, Salmonella typhimurium, Staphylococcus aureus* and *Streptococcus faecalis* and anti-fungal studies in Sabouraud's Dextrose agar as base against fungi *Candida albicans* and *Aspergillus niger* are of considerable amount. Antimicrobial analysis data perceived for **R1** and **R2** are presented in Table 6.

Table 6. *In vitro* antimicrobial studies data.

Microorganisms	Control	R1	R2	Ciprofloxacin/ Ketoconazole
Zone of inhibition in mm for bacteria				
Staphylococcus aureus	-	07	15	35
Streptococcus faecalis	-	10	-	28
Escherichia coli	-	09	10	35
Salmonella typhimurium	-	08	09	30
Zone of inhibition in mm for fungi				
Candida albicans	-	09	10	15
Aspergillus niger	-	07	10	27

Fungi *Candida albicans* growth is prevented by both compounds **R1 (**60 %**)** and **R2 (**66 %**).** Above results may lead to the development of new formulation of antifungal agent up on more specific research by pharmacist [23]. Growth of fungi *Aspergillus niger* is also restricted to an extend of **R1** (26 %) and **R2** (37 %). Level of preventive nature against all four bacteria by **R1**(20 %, 36 %, 26 % and 27 %) and **R2**(43 %, 0 %, 29 % and 30%) are on par with the value obtained for standard material Ciprofloxacine. Further it is clear that **R2** is not successful to avoid the progress of *Streptococcus faecalis.* Schiff base compound 5-(benzylideneamino)-3-(4-methoxyphenylamino)-N-phenyl-1H-pyrazole-4-carboxamides, found to resist multidrug-resistant bacteria (MDRB) [36]. Some of the materials reported earlier showed higher antibacterial activity than ciprofloxacin [37]. Antifungal activity of cinnamyl Schiff bases [38] and resistivity of sulphonamides Schiff bases against multidrug-resistant fungi [39] also expose the antimicrobial activity of Schiff base compound.

Molecular docking studies

The driving force operating between the guest- host entities of drug molecule and targeted proteins of microorganisms is predicted using the molecular docking software. Relevant proteins employed in molecular docking studies for fungi are 3K4Q- *Aspergillus niger,* 6TZ6- *Candida albicans,* and bacteria are 6KVQ - *Staphylococcus aureus,* 4YXB- *Salmonella typhimurium,* 1PTF- *Streptococcus faecalis* and 7BU2- *Escherichia coli.* The data obtained are presented in Table 7. The 3D and 2D structural binding views of **R1** and **R2** are given in figures 18 (**(a)** to **(f)**) and 19 (**(a)** to **(f)**). The binding energy values calculated for R1 against fungi protein falls between - 6.99 to -7.63 kcal mol^{-1}. For **R2** it is -3.79 and -6.99 kcal mol^{-1}, which exposes that both ligands are capable of fighting against fungi *Aspergillus niger* and *Candida albicans.*

Table 7. Results obtained in molecular docking studies.

PDB	Free binding energy, kcal mol^{-1}		R1		R2	
	R1	R2	Hydrogen bonds with receptor amino acids	Distance(Å)	Hydrogen bonds with receptor amino acids	Distance(Å)
1PTF	-4.63	-4.01	4-LYS 5-GLU 6-PHE	3.94 3.78 3.19	6-PHE ALA-57	3.14 3.28
3K4Q	-7.63	-3.79	32-PHE 23-HIS 365-ASN 373-SER	3.91 3.58 3.86 3.44	32-PHE 365-ASN	3.18 3.38
4YXB	-4.69	-5.07	195-LEU 196-ILE 215-ILE	3.43 3.17 3.27	26-ALA 27-ASP 28-ILE 29-PRO	3.74 3.22 3.91 3.55
6KVQ	-8.28	-2.14	22-GLY 131-VAL 103-SER	3.28 3.66 3.16	192-GLN 193-GLY ASN-263	3.96 3.38 3.42
6TZ6	-6.99	-6.99	44-LYS 238-THR	2.89 3.06	40-PHE 58-GLN 97-TYR	2.78 3.86 3.75
7BU2	-6.01	-2.42	282-LEU 284-GLY 291-PHE	3.55 3.72 3.13	329-ALA 332-ARG	3.96 3.47

Fig. 18. 3D and 2D view binding of **R1** with **(a)** 1PTF, **(b)** 3K4Q, **(c)** 4YXB, **(d)** 6KVQ, **(e)** 6TZ6, **(f)** 7BU2.

Fig. 19. 3D and 2D view binding of **R2** with **(a)** 1PTF,**(b)** 3K4Q, **(c)** 4YXB, **(d)** 6KVQ, **(e)** 6TZ6, **(f)** 7BU2.

Conclusion

High reactivity associated with ferrocene and its derivatives prevents the synthesis of unsymmetrical Schiff bases starting with a mixture of aromatic aldehyde, ferrocene aldehyde and amines (aliphatic or aromatic). Our attempts to prepare such type of Schiff bases resulted with　unsymmetrical compounds *N'*1-((*E*)-4-(Nitro)benzylidene)-*N'*4-((*E*)-2-(ferrocenylidene)succinohydrazide　　and　　*N'*1-((*E*)-4-(Dimethylamino)benzylidene)-*N'*4-((*E*)-2-(ferrocenylidene)succinohydrazide. FTIR, proton NMR and Mass spectrum analysis endorse the formation of above materials. UV-Visible spectral analysis coupled with titration reveals the multi metal ion sensing capacity of newly synthesized sensors. From cyclic voltammetry studies, it is observed that the power of sensing changes with the change in concentration of targeted metal ions. Molecular docking and *in vitro* studies expose the antifungal activity of compound **R1** and **R2** against *Candida albicans*.

Acknowledgments

References

1. Osório, M. V.;, Marques, S. S.; Oliveira, H. M.; Barreiros, L.; Segundo, M. A. *J. Food Compos. Anal.* **2016**, *45,* 141–146. DOI: https://doi.org/10.1016/j.jfca.2015.10.007.
2. Frank, C. B.; Scott, R. B.; Kiril D. H.; Russell, G. B.; Evan, Taylor, D. A.; Hoffman. *Maced. J. Chem. Chem. Eng.* **2020**, 39, 119–127. DOI: https://doi.org/10.20450/mjcce.2020.
3. Chiu-Hsien, Wu.; Guo-Jhen, J.; Kai-Wei, C.; Zu-Yin ,D.; Yu-Ning, L.; Kuen-Lin, C.; Chien-Chung, J. *Sensors.* **2018**, *18*, 163-171. DOI: https://doi.org/10.3390/s18010163.
4. Mayer, M.; Baeumner, A. J. *Chem. Rev*. **2019**, *119*, 7996–8027. DOI; https://doi.org/10.1021/acs.chemrev.8b00719.
5. Johnson, D. A.; Curtis, M. R.; Wallace, J. K. *Chemosensors*. **2019**, *7*, 1–48. DOI: https://doi.org/10.3390/chemosensors7020022.
6. Vedamalai, M.; Kedaria, D.; Vasita, R.; Moric, S.; Gupta, I. *Dalton Trans*. **2016**, *45*, 2700–2708. DOI: https://doi.org/10.1039/C5DT04042F.
7. Qi, X.; Jun, E. J.; Xu, L. *J. Org. Chem*. **2006**, *71*, 2881-2884. DOI: https://dx.doi.org/10.1021/jo052542a.
8. Ingle, A. P.; Paralikar, P.; Shende, S.; Gupta, I.; Biswas, J. K.; da Silva Martins, L. H.; Rai, M. *Biomedical Applications of Metals*. **2018**, 95–112. DOI: https://doi.org/10.1007/978-3-319-74814-6_4
9. Desguin, B.; Fellner, M.; Riant, O.; Hu, J.; Hausinger, R.P.; Hols, P.; Soumillion, P. *J. Biol. Chem*. **2018**, *293*, 12303–12317. DOI: https://doi.org/10.1074/jbc.RA118.003741.
10. Genchi, G.; Carocci, A.; Lauria, G.; Sinicropi, M. S.; Catalano, A; *Int. J. Environ. Res.Public Health.* **2020***, 17,* 679.DOI: https://doi.org /10.3390/ijerph17030679.
11. Zambelli, B.; Uversky, V.N.; Ciurli, S. *BBA Proteins Proteom*. **2016**, *1864*, 1714–1731.
12. Mehrdad, R. R.; Mehravar R. R.; Sohrab, K.; Ali-akbar, M. *Caspian J. Intern Med* .**2017**, *8*,135-145. DOI: https://doi.org/10.22088/cjim.8.3.135

13. Zhu, W.; Richards, N. G. J. *Essays Biochem.* **2017**, *61,* 259–270. DOI: https://doi.org/10.1042/ebc20160070

14. Freeland-Graves, J. H.; Mousa, T. Y.; Kim, S. *J. Trace Elem. Med. Biol.,* **2016**, *38,* 24–32. DOI: https://doi.org/10.1016/j.jtemb.2016.05.004.

15. Hariharan, G.; Purvaja, R.; Ramesh, R. *Environ. Toxicol.* **2016**, *31*, 24–43. DOI: https://doi.org/10.1002/tox.22019.

16. Wani, A. L.; Ara, A.; Usmani, J. *Interdiscip. Toxicol.* **2015,** *8, 55–64.* DOI: https://doi.org/10.1515/intox-2015-0009.

17. Gidlow, D. A. *Occup. Med.* **2015**, *65,* 348–356. DOI: https://doi.org/10.1093/occmed/kqv018.

18. Dubar, F.; Egan, T. J.; Pradines, B.; Kuter, D.; Ncokazi, K. K.; Forge, D.; Biot, C. *ACS Chemical Biology,* **2011**, *6,* 275–287.DOI: https://doi.org/10.1021/cb100322v.

19. Gupta, S. R.; Mourya, P.; Singh, M. M.; Singh, V. P. *J. Organomet. Chem.* **2014**, *767,* 136–143. DOI: https://doi.org/10.1016/j.jorganchem.2014.05.

20. Hranjec, M.; Starčević, K.; Pavelić, S. K.; Lučin, P.; Pavelić, K.; Karminski Zamola, G. *Eur. J. Med. Chem.* **2011**, *46*, 2274–2279. DOI: https://doi.org/10.1016/j.ejmech.2011.03.008.

21. Mohamed, G. G.; Mahmoud, W. H.; Diab, M. A.; El-Sonbati, A. Z.; Abbas, S. Y. *J. Mol. Struct.* **2019**, 1-15. DOI: https://doi.org/10.1016/j.molstruc.2019.01.00.

22. Farouk, K., Mohamad, K. C.; Wail Al. Z. *ISRN Org. Chem.* **2012**, *8*, 208284. DOI: https://doi.org/10.5402/2012/208284.

23. Bagamboula, C.F.; Uyttendaele, M.; Debevere, J. *Food Microbiol..* **2004**, *21*, 33-42. DOI: https://dx.doi.org/10.1016/s0740-0020(03)00046-7.

24. Morris, G.M.; Huey, R.; Lindstrom, W.; Sanner, M. F.; Belew, R. K.; Goodsell, D.S.; Olson, A.J. *J. Comput. Chem.* **2009**, *30*, 2785- 2791. DOI: https://dx.doi.org/10.1002/jcc.21256.

25. Gryaznova, T. P.; Katsyuba, S. A.; Milyukov, V.A.; Sinyashin, O.G. *J. Organomet. Chem.* **2010**, *695***, 2586- 2595. DOI: https://dx.doi.org /10.1016/j.jorganchem.2010.08.031.

26. Mandewale, M. C.; Bapu,T.; Nivid , Y.; Ram Jadhav A. N.; Yamgar, R. *J. Saudi Chem. Soc.* **2016**, 22, 218-228. DOI: https://dx.doi.org/10.1016/j.jscs.2016.04.003.

27. Berna,C *Periodcals Eng. Nat. Sci.* **2017,** 5, 237-244. DOI: https://dx.doi.org/10.21533/pen.v5i2.139

28. Benramdane, R.; Benghanem, F.; Aliourari.; Keraghel, S.; Bouet, G. *J. Coord. Chem*, **2015**, *68*, 560-572. DOI: https://dx.doi.org/10.1080/00958972.2014.994514.

29. Jinghui, C.; Xiaofeng, M.; Yuhui, Z.; Jiaoyan, L.; Xiangge, Z.; Haifeng, X. *Inorg. Chem.* **2014**, *53*, 3210−3219. DOI: https://doi.org/10.1021/ic5000815

30. Rampal, P.; Rakesh Kumar, G.; Mohammad, S.; Biswajit, M.; Arvind, M.; Daya Shankar, P. *Inorg. Chem.* **2012**, *51*, 298−311. DOI: https://doi.org/10.1021/ic201663m.

31. Schrage, B. R.; Zhao, Z.; Boika, A.; Ziegler, C. J. *J. Org. Chem.* **2019**, *897,* 23–31.DOI: https://doi.org/10.1016/j.jorganchem.2019.06.023.

32. Kamatchi, P.; Selvaraj, S.; Kandaswamy, M. *Polyhendron.* **2005**, *24*, 900-908. DOI: https://doi.org/10.1016/j.poly.2005.02.012.

33. Kamal, A S.; Kuma.r, S.; Kumar, V.; Mahajan, R.K. *Sens. Actuators B*. **2015**, *22*, 370-378. DOI: https://dx.doi.org/10.1016/j.snb.2015.06.147.

34. John, M. W. S.; Jura, W. H. *Can. J. Chem.* **1967**, 45, 2375-2384. DOI: https://doi.org/10.1139/v67-385.

35. Rebecca, Y. L.; Allen, J. B. *J. Phys. Chem. B.* **2003,** *107,* 5036-5042. DOI: https://doi.org/10.1021/jp034578h.

36. Hassan, A.S.; Askar, A.A.; Nossier, E.S.; Naglah, A.M.; Moustafa, G.O.; Al-Omar, M.A. Molecules. **2019**, *24*, 3130. DOI: https://doi.org/10.3390/molecules24173130.

37. Pozzi, C.; Ferrari, S.; Cortesi, D.; Luciani, R.; Stroud, R.M.; Catalano, A.; Costi, M.P.; Mangani, S. Acta Cryst. D **2012**, *68*, 1232–1241. DOI: https://doi.org/10.1107/S0907444912026236.

38. Magalhães, T. F. F.; da Silva, C. M.; Dos Santos, L. B. F.; Santos, D. A.; Silva, L. M.; Fuchs, B. B.; Mylonakis, E.; Martins, C. V. B. *Lett. Appl. Microbiol.* **2020**, *71*, 490–497. DOI: https://doi.org/10.1111/lam.13356.

39. Hamad, A.; Chen, Y.; Khan, M. A.; Jamshidi, S.; Saeed, N.; Clifford, M.; Hind, C.; Sutton, J. M.; Rahman, K.M. *Microbiol. Open.* **2021**, *10*, e1218. DOI: https://doi.org/10.1002/mbo3.1218.